ADVANCED FUNCTIONAL MATERIALS
www.afm-journal.de

Efficient Piezoelectric Energy Harvesters Utilizing (001) Textured Bimorph PZT Films on Flexible Metal Foils

*Hong Goo Yeo, Xiaokun Ma, Christopher Rahn, and Susan Trolier-McKinstry**

Extracting energy from low vibration frequencies (<10 Hz) using piezoelectric energy harvester promises continuous self-powering for sensors and wearables. The piezoelectric compliant mechanism (PCM) design provides a significantly higher efficiency by fostering a uniform strain for its 1st mode shape, and so is interesting for this application. In this paper, a PCM energy harvester with bimorph $Pb(Zr,Ti)O_3$ (PZT) films on Ni foil deposited by rf magnetron sputtering is shown to have high efficiency and large power for low frequency mechanical vibration. In particular, {001} textured PZT films are deposited on both sides of polished Ni foils with (100) oriented $LaNiO_3$ seed layers on HfO_2 buffer layers. The performance of PCM with an active area of 5.2 cm^2 is explored for various excitation accelerations (0.02–0.16 g [g = 9.8 m s^{-2}]) around 6 Hz. The PCM device provides a power level of 3.9 mW cm^{-2} g^2 and 65% mode shape efficiencies.

1. Introduction

There are numerous applications where it would be desirable to track system responses over time, ranging from wearable sensor devices for health and fitness, to emplaced wireless sensors for infrastructure and building monitoring. In most cases, such devices require periodic recharging or replacement of batteries. However, with the on-going introduction of low power electronics, opportunities are being opened to replace batteries with solar, thermal, and mechanical harvesters. Piezoelectric energy harvesters, can extract energy from human activities such as walking, breathing, and typing, or from motion of walls, air ducting, or bridges without limitations on the location and time of use (e.g., indoors or at night).[1,2] However, mechanical energy harvesting is faced by challenges such as weak base excitations with low natural frequency (<10 Hz)[3,4] and fragile structures that are susceptible to shock. To overcome these challenges, the piezoelectric energy harvester should have high efficiency, be flexible, and have a low resonance frequency with wide bandwidth. Numerous methods to improve the output power density and reduced resonance frequency have been explored, including advanced mechanical design,[5] maximizing intrinsic piezoelectric materials properties,[6,7] and using a flexible passive layer.[8,9]

In the last decade, microelectromechanical (MEMS) energy harvesters based on piezoelectric materials such as AlN and $Pb(Zr,Ti)O_3$ (PZT) have been studied for use in harvesting energy from small amplitude, mechanical vibration.[10–12] Improving the piezoelectric material for a piezoelectric energy harvester (PEH) can be pursued via an energy harvesting figure of merit (FoM). The maximum extractable electric power generated at the resonance frequency of a $e_{31,f}$ mode cantilever structure is[13,14]

$$\text{Power}_{\max} = \frac{1}{4}\left(\frac{e_{31,f}^2}{\varepsilon_r \varepsilon_0} \cdot \frac{m}{Y}\right)\frac{a^2}{\omega} \quad (1)$$

where m is mass, ω is angular frequency, Y is Young's modulus, ε_0 is vacuum permittivity, and a is the acceleration. The in-plane piezoelectric coefficient ($e_{31,f}$) and the relative permittivity (ε_r) control the energy harvesting FoM = $(e_{31,f})^2/\varepsilon_r$ when the mechanical energy is stored in the passive layer. The orientation of the PZT grains strongly influences the figure of merit.[7,15] In particular, strongly (001) oriented PZT films, which have a significant fraction of the ferroelectric polarization directed out-of-plane, have large FoM.[16]

From the standpoint of improving the toughness and reliability of the piezoelectric energy harvester, a metal foil is preferable compared to Si, the typical substrate for MEMS.[17] Moreover, thin metal foils enable low resonance frequencies without etching, and are easily machined. Morimoto et al.[8] reported a cantilever piezoelectric energy harvester using epitaxial PZT thin films transferred onto stainless steel that shows output power of 5.3 μW at 5.0 m s^{-2} and 126 Hz without a proof mass. In much the same way, $(Na_{0.5}K_{0.5})NbO_3$ (NKN) piezoelectric thin films coated on Ni-based metal foils were investigated for vibration energy harvesters.[18] Another benefit of using metal substrates for PEH is that copper and nickel have larger thermal expansion coefficients than many perovskite films. This produces compressive stresses in the tetragonal PZT film on cooling, increasing the volume fraction of the out-of-plane polarization direction.[19] Thus, high compressive stresses in {001} PZT films give rise to an improved FoM for energy harvesting.[7,19–21]

Typical PEH designs use a fixed-free cantilever beam configuration with or without a proof mass. While fixed-free

H. G. Yeo, Prof. S. Trolier-McKinstry
Materials Science and Engineering Department
and Materials Research Institute
The Pennsylvania State University
University Park, PA 16802, USA
E-mail: stmckinstry@psu.edu
X. Ma, Prof. C. Rahn
Department of Mechanical and Nuclear Engineering
The Pennsylvania State University
University Park, PA 16802, USA

DOI: 10.1002/adfm.201601347

cantilevers undergo larger strains compared to bridges, for the same input force, the strain distribution along the piezoelectric beam is not uniform.[22] Thus, it would be preferable to improve the efficiency of the first mode shape to maximize power by uniformly straining PZT films while preventing overstrain near the clamping points. Ma et al.[23] proposed a piezoelectric compliant mechanism (PCM) design for PEH that leads to a much more uniform strain distribution. Simulations for the compliant mechanical design suggested that this configuration can reach 100% mode shape efficiency by curving the beam into a perfect parabola, compared to 24% efficiency for a cantilever beam.[23] PZT films on metal foils are well suited for this design. To achieve a high efficiency piezoelectric energy harvester operated at a low resonance frequency and acceleration level, this study focuses on using bimorph textured PZT films on Ni foil in a PCM harvester. The PZT films have stress-tailored domain structures that provide efficient electromechanical conversion with high FoM. Bimorph piezoelectric energy harvesters using piezoelectric ceramics are well known,[24] but there is little literature on implementing this idea in films. Indeed, the deposition of PZT film in a bimorph structure on a released structure on a Si substrate is very difficult using typical microfabrication processes.[2,25]

A PCM energy harvester consists of three parts, as shown schematically in **Figure 1**. First, the bimorph PZT beam electroded on the major surfaces converts mechanical energy to electrical energy. A two part rigid frame is employed; the U-shaped frame elements are connected to the complaint hinges which ideally have zero stiffness, to make a single structure. A third compliant hinge, with a torsional spring stiffness K_1, connects the PZT beam to the rigid frame on the side with the proof mass. In the design of the PCM, the shape of the deflected PZT beam length can be adjusted by the values of the spring constant K_1 and equivalent mass as described elsewhere.[23] In this work, a PCM device was fabricated from {001} oriented PZT films on Ni foils, epoxy plates for the rigid frame, and 75 µm thick polyethylene terephthalate (PET) films with low stiffness for the compliant hinges. The output power of the fabricated PCM device was evaluated as a function of resonance frequency, acceleration level, and load resistance. Additionally, the displacement distribution along the PZT beam was characterized.[23]

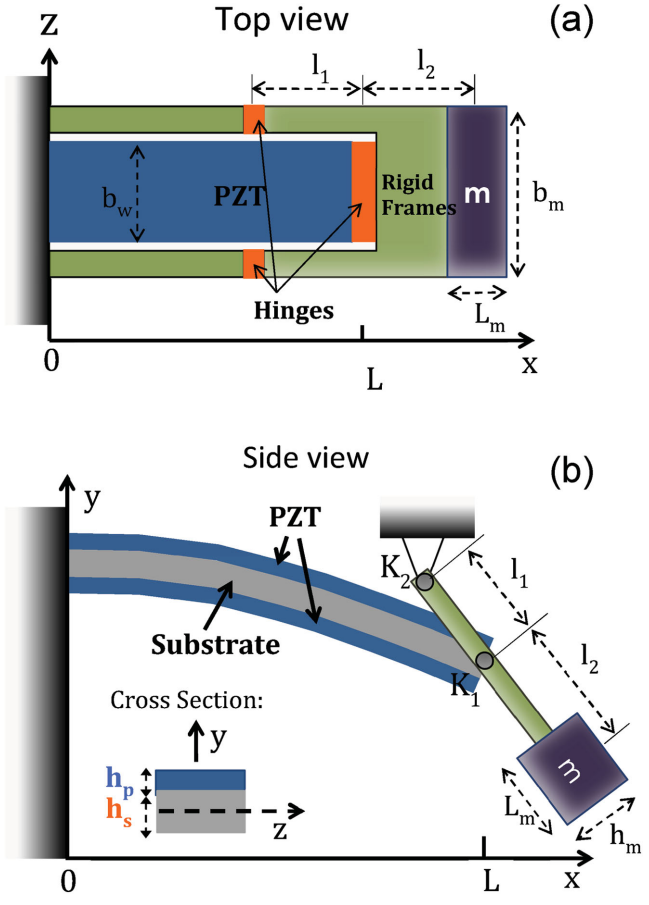

Figure 1. Schematic a) top and b) side views of PCM.

2. Results and Discussion

2.1. Fabrication of Piezoelectric Compliant Mechanism Energy Harvester

To demonstrate the PCM design energy harvester, (001) textured PZT thin films on Ni foils were prepared on a sol-gel $LaNiO_3$ (LNO) seed layer coated on top of a HfO_2 buffer layer that served to suppress oxidation of the Ni foil during annealing in air, as shown schematically in **Figure 2**a. The buffer and seed layers were deposited on both sides of pretreated 25 µm thick Ni foils (Aldrich Aesar 99.99%) as described elsewhere.[19] PZT layers were fabricated by rf magnetron sputtering using a 10% Pb excess and 1% Mn doped $Pb(Zr_{0.52}Ti_{0.48})O_3$ target under the conditions shown in Table S1 of the Supporting Information.[26] Mn doping provided a lower dielectric permittivity following poling than could be achieved in undoped PZT as a result of an internal bias; this increased the FoM of the energy harvester.[7] To achieve (001) preferred orientation in PZT films by room temperature sputtering, it is necessary to control nucleation and growth during crystallization. Ideally, heterogeneous nucleation sites on (100) oriented LNO enable (001) oriented PZT films.[19,27,28] In practice, it was found that when amorphous PZT films thicker than 0.5 µm were crystallized, surface nucleation was observed before completion of the growth of columnar grain at interface nucleation sites.[29] Thus, in order to maintain orientation, 0.5 µm thick PZT layers were sputtered at room temperature and post-annealed by rapid thermal annealing (RTA) iteratively to reach the desired thickness (≈3 µm). Each 0.5 µm PZT layer was grown on alternative sides of the Ni to keep the samples flat during crystallization and suppress large curvature after crystallization due to thermal expansion mismatch between PZT films and Ni foil.[30,31] Figure S1 of the Supporting Information shows pictures of typical unimorph and bimorph PZT films on Ni foil.

Figure 3 shows the X-ray diffraction (XRD) patterns of upper and lower PZT films on Ni. Strongly {001} textured PZT films on both side of Ni foils were achieved without second phase, as was earlier reported for chemical solution deposited PZT thin films on Ni foils.[19] Based on the crystallinity of both PZT film, low dielectric constant ($\varepsilon_r \approx 210$) and large remanent

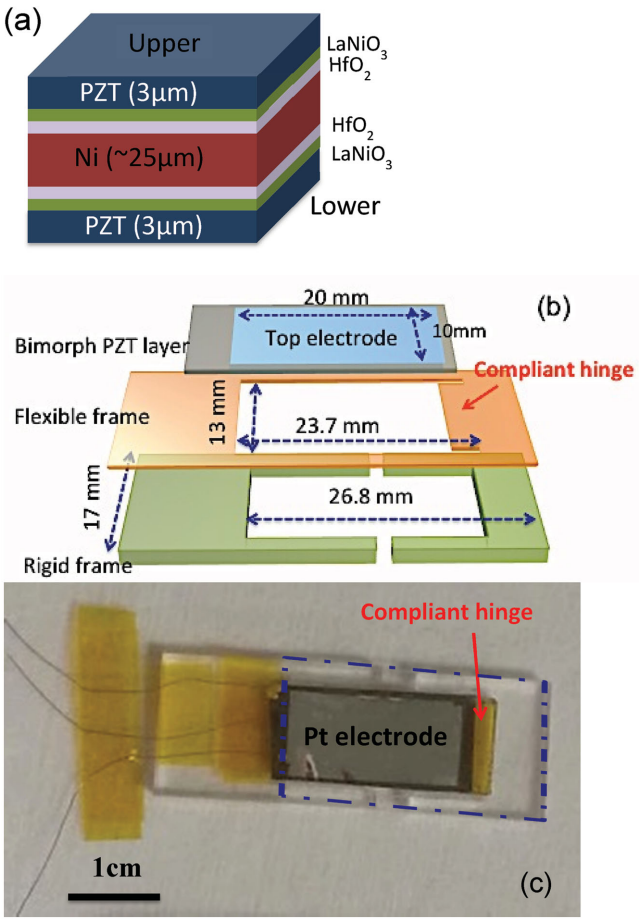

Figure 2. a) Schematic of bimorph PZT film stacks with $LaNiO_3$ and HfO_2 layers on Ni. b) Schematic illustration of each part; bimorph PZT beam with top electrode, flexible, and rigid frame with dimensions. c) Prototype PCM device integrated with bimorph PZT film, PET hinge, and acrylic plates.

polarization ≈40 μC cm^{-2} were observed for both PZT layers in Figure S5 of the Supporting Information. The low dielectric constant is caused by large of c-domain population and pores[19,32] and enhances the FoM of the PEH. This paper is the first report of deposition of high figure of merit bimorph PZT films on metal foils for piezoelectric energy harvesters. Table S2 of the Supporting Information shows parameters for each part of the PCM with material properties of the bimorph PZT films and Ni substrate. Following optimization of parameters from the PCM model, rigid frames were laser cut from 3 mm thick epoxy. The compliant hinges were made from 75 μm thick PET with the addition of Kapton tape layers to reach the optimum stiffness K_1. Finally, parts were combined by cyanoacrylate glue. To connect the bimorph PZT beam to the center hinge, 1.5 mm of the beam was not covered with a Pt electrode in Figure 2b. A 3 mm distance separated the two rigid frames; ideally this should have zero stiffness (K_2). A photograph of the assembled device is given in Figure 2c. The active area of the fabricated energy harvester is around 5.2 cm^2 (blue box in Figure 2c). The device was designed for 4.95 Hz resonance frequency; details on the modeling approach are provided elsewhere.[23]

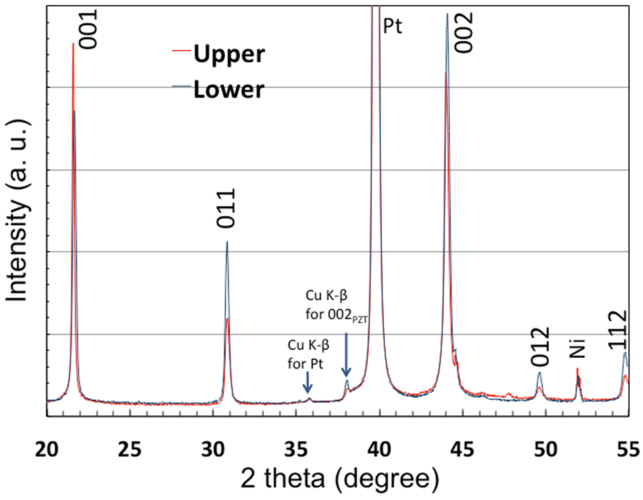

Figure 3. X-ray diffraction (XRD) scan of crystallized upper and lower 1%Mn doped PZT(52/48) films, respectively, by sputtering on $LaNiO_3$/HfO_2/Ni/HfO_2/$LaNiO_3$ substrate (PANalytical X'pert).

2.2. Performance of Piezoelectric Compliant Mechanism Energy Harvester

The performance of the PCM energy harvester was characterized using a laser Doppler vibrometer (OFV-534 Compact Sensor head, Polytec), an electrodynamic shaker and LabVIEW data acquisition system (Figure S2a,b, Supporting Information).[23] The PCM was mounted hanging vertically to a shaker table as shown in Figure S2 of the Supporting Information. To measure the performance of the PCM device, the top electrode of the upper and lower PZT layers were wired in series and connected to a resistor box to tune the load resistivity. The sinusoidal excitation base excitation was swept from 0 to 30 Hz in order to understand the dynamic behavior, including the resonance frequency, the mechanical quality factor (Q), and damping ratio (ζ). A video showing device operation under resonant excitation is shown in Video S1 of the Supporting Information.

Figure 4 shows the theoretical and experimental power sensitivity as a function of frequency. The measured first resonance frequency was ≈6.3 Hz, in reasonable agreement with the theoretical model. It is noted that although the model presumes zero stiffness for the hinges, the finite stiffness of the PET film leads to some deviation between the measured and modeled resonance frequencies. The mechanical quality factor calculated using the half power method: $Q = f_r/(f_b - f_a)$ (where f_r is resonance frequency and $f_b - f_a$ is the bandwidth at the half-maximum amplitude was 24.5.[25] The mechanical damping ratio, $\zeta = (f_b - f_a)/2f_r$, was 2.07%.

Figure 5a shows the voltage and power of the PCM device as function of the external load resistance (R) connected in parallel with the device and varying from 1000 Ω to 1000 kΩ to figure out optimum load resistance, for steady-state excitation at 6.3 Hz. The maximum voltages ($V_{max} = V_{pk-pk}/2$) were measured as a function of load resistance to determine the optimum load resistance for maximum power transfer ($P_{max} = V_{max}^2/R$). The modeled optimal load resistance (R_{opt}) was 239.6 kΩ at

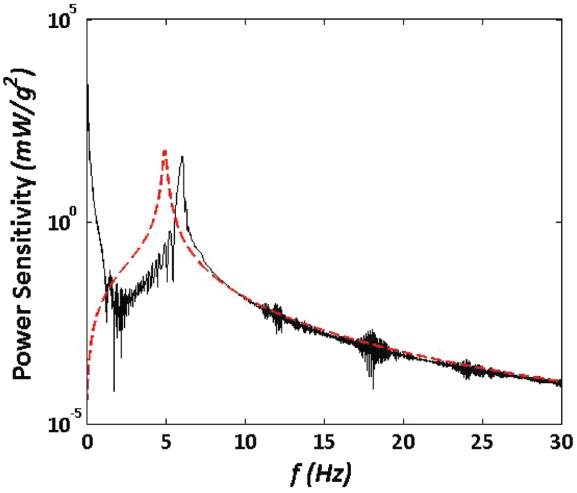

Figure 4. Dynamic power sensitivity as a function of frequency for PCM device (black line) and theory (red line) at the load resistance of 330 kΩ.

0.045 g [g = 9.8 m s^{-2}] for series connection. The experimental results gave an optimal load resistance around 330 kΩ; at this point the generated power reached a maximum of 113 μW and a peak-to-peak voltage of 12.2 V (red dot and line) for series connection at an acceleration level of 0.08 g. Figure 5b shows the generated electric maximum power of PCM device versus acceleration. The experimental output power increases with increasing base excitation for amplitudes above 0.05 g.

On the other hand, the generated power significantly dropped under 0.05 g. It is believed that the drop-off at low excitations is due to local curvature in the PZT-coated beam. As a result, a finite input force is required to excite the full length of the PZT beam. Even though PZT films were coated on both sides of the Ni foil to compensate for stresses associated with thermal expansion mismatch during cooling, it is challenging to fabricate perfectly flat PZT beams without partial buckling. This local curvature also degrades the resonant mode shape at higher acceleration levels. It is also possible that the damping ratio increases.

The output voltage of the upper and lower PZT beams at an excitation level of 0.09 g is, respectively, shown in Figure 5c. Under 0.09 g acceleration, the maximum output power generated from the upper and lower beams was around 85 μW at load resistances of 100 and 220 kΩ, respectively (see Figure 5c). In principle, the output voltage could be scaled up when both layers are connected in series. However, the measured power output from both PZT layers (P_{max} = 141 μW) falls below the sum of the powers from the individual PZT layers. It is believed that small differences in thickness, dielectric permittivity, and/or the volume of c-domains of the two PZT layers resulted in mismatched optimum load resistances, decreasing the output power slightly.[32]

As designed, the first mode shape of the PCM is close to parabolic, enabling a uniform strain distribution along the beam direction. In **Figure 6**, the experimental first mode shapes measured by for various excitation levels are plotted along with the theoretical first mode shape of the PCM and a proof mass cantilever energy harvester. The displacement of the PCM device at each point along the beam from the clamped point to the tip

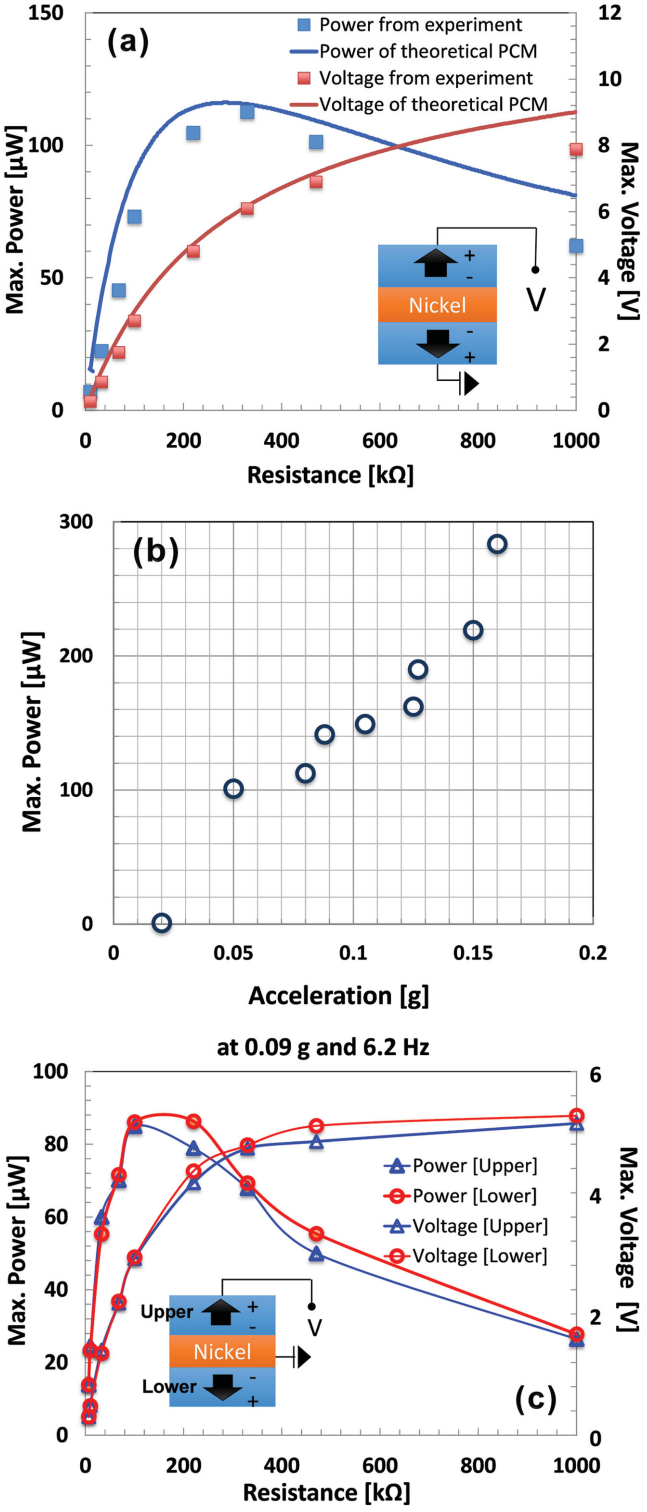

Figure 5. a) Maximum output voltage (red) and power (blue) as a function of external load resistance for PCM device (dots) and theory (lines). [Inset: Series poling configuration for bimorph PZT layers. Arrows represent poling direction through PZT layers.] b) Maximum output power versus acceleration amplitude. c) Maximum output voltage and power for upper (blue triangle) and lower (red circle) PZT layers, respectively, as a function of external load resistance.

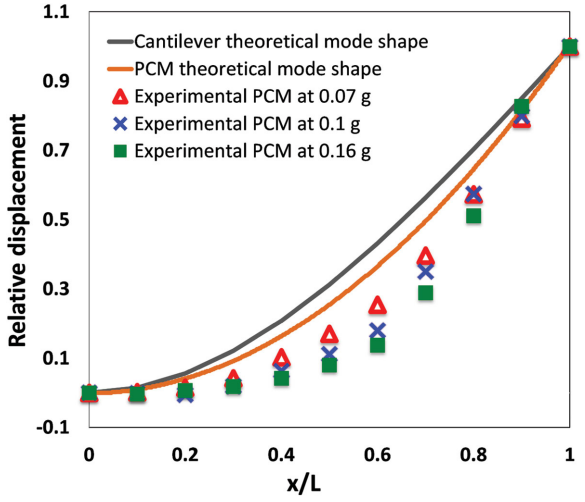

Figure 6. Normalized first mode shape along the relative distance of experimental PCM device at various excitation amplitudes, theory (orange), and proof mass cantilever theory (gray).

of PZT beam was measured using a laser vibrometer. Flexible reflective tape was fixed to the PZT beam in order to detect the signals. It can be seen that the first mode shape of the PCM at low acceleration levels is relatively close to a parabola, although significant deviation is observed for higher acceleration levels. The origin of the nonuniform strain distribution of PCM device was also explored. Figure S3 of the Supporting Information shows the displacement responses along the PZT beam length.

We observed a linear/symmetric response to a sinusoidal input vibration as expected from a theoretical model having no initial asymmetrical deformation near the clamped end of the beam (x = 0.1); this is shown in Figure S3a of the Supporting Information. However, 30%–60% along the beam length, strongly nonlinear displacements were observed at 0.07 g. This was attributed to some initial beam curvature as marked by the green box in Figure S3b of the Supporting Information. Also, the bending response to resonance excitation is shown in Video S1 of the Supporting Information.

Table S3 of the Supporting Information shows the output power and power density (in μW cm^{-2} g^{-2}, where g is the acceleration) of PCM device at various acceleration levels compared with the modeled output at 0.05 g. The output power increased with the acceleration over the whole measured range, reaching a maximum power of 284 μW at 0.16 g. The power density decreased with increased acceleration level, due to degradation of the uniformity of strain distribution. For a maximum strain of 0.1% corresponding to the acceleration level of 0.1 g in the PZT, the maximum power of 149 μW from PCM device shows 65% mode shape efficiency compared to theoretical estimates. This is much higher than the efficiency of normal cantilever with a proof mass.[23] It is anticipated that up to 100% mode shape efficiency could be achieved as initial curvature along PZT is eliminated beam along with clamping at the end of the PZT beam.

2.3. Comparison of Piezoelectric Energy Harvester Performance

A comparison of the power density of various reported piezoelectric energy harvesters is shown in **Table 1**. For the 3 μm thick bimorph PZT film on Ni foil, under 0.05 g acceleration, the root mean square (RMS) power of the device is 51 μW at ≈6 Hz. This significantly outperforms all of the MEMS devices using piezoelectric films. This is the first report that demonstrates both a low high resonance frequency and high power density, respectively, in a small structure. Furthermore, normalized to the resonance frequency, the power density exceeds all other reports, including the average of the two branches reported by Leadenham et al. for a strongly nonlinear harvester, which may be not allowed for small electronic devices.[33] It is noted that the PCM devices using textured bimorph PZT beams demonstrate

Table 1. Comparison of recently reported resonant based piezoelectric energy harvesters.

Reference	Active material, mode	Device area [cm^2]	Acceleration [g]	Frequency [Hz]	Power$_{rms}$ [μW]	Power density [μW cm^{-2} g^{-2}]	Power density/f_r [μW Hz^{-1} cm^{-2} g^{-2}]
Shen[34]	PZT film sol-gel, d_{31}	0.0256	2	462.5	2.15	21	0.05
Morimoto[8]	(001) PZT on stainless steel, d_{31}	0.925	0.5	126	5.3	22.9	0.18
Kim[35]	Cymbal type w/high-g PZT ceramic	6.6	9.4	100	19500	33.4	0.334
Kim[18]	NKN on Ni-rich foil, d_{31}	0.1	0.5	128	1.75	70	0.546
Andosca[36]	Sputtered AlN d_{31}	0.653	1	58	64	98	1.69
Durou[37]	Bulk PZT-5H thin-bonded, d_{31}	0.894	0.2	76	13.9	388.7	5.11
Zawada[38]	PZT thick film, d_{31}	0.75	0.102	205	3.78	481	2.35
Aktakka[39]	Bonded and Thinned Bulk-PZT5A d_{31}	0.49	0.1	167	2.74	559.2	3.35
Ricart[40]	5.6 μm AlN, d_{31}	3.38	0.18	155	165	1507	9.72
Leadenham[33]	M-shaped beam w/four piezoelectric patches	55.88	0.06	14.5	2610[a)]	12974	895
					14[b)]	70	4.83
Ma[23]	Compliant design using PVDF	5.2	0.01	5.13	0.062	119.2	23.2
PSU compliant	3 + 3 μm bimorph PZT film on Ni d_{31}	5.2	0.05	6	50	3887	617

[a)]High-energy branch (up frequency sweep); [b)]Low-energy branch (down frequency sweep).

excellent power density (≈3.9 mW cm^{-2} g^{-2}) at 6 Hz relative to other reports due to the combination of advanced design and the excellent characteristics of bimorph PZT films with a high figure of merit on Ni foil.

3. Conclusions

In conclusion, a piezoelectric compliant mechanism mechanical energy harvester providing comparatively uniform strain along the beam length was successfully fabricated using bimorph PZT films on flexible Ni foils. (001) textured 3 µm thick PZT films were coated on both sides of Ni foil (PZT/$LaNiO_3$/HfO_2/Ni/HfO_2/$LaNiO_3$/PZT) by rf-sputtering with post annealing. The bimorph PZT beam exhibits approximately twice the power output of a unimorph PZT layer and avoids large transverse curvature along the beam produced by thermal expansion mismatch. A 6 Hz PCM device utilizing a 2 cm × 1 cm PZT beam generated a maximum voltage and power of 7 V and 149 µW, respectively, at 0.1% strain limit at 0.1 g acceleration level. Large power densities (3.9 mW cm^{-2} g^{-2}) and higher mode shape efficiencies (65%) relative to available reports on piezoelectric energy harvesters were shown.

4. Experimental Section

Fabrication of the Buffer and Seed Layers on Ni Foil: For fabrication of bimorph PZT beams, the amorphous HfO_2 passivation layer was coated on both sides of the Ni simultaneously, by propping the Ni foil at an angle to the sample stage using glass spacers; atomic layer deposition was utilized at 200 °C for 300 cycles (0.95 Å per pulse). 0.2 M $LaNiO_3$ chemical solutions based on a 2-methoxyethanol (2MOE) solvent were spin-coated on one side of the Ni foil at a time and pyrolyzed on a hot plate in air. Each $LaNiO_3$ layer was crystallized by RTA at 700 °C in air; these processes were repeated five times to fabricate a 100 nm thick (100) oriented LNO layer. The other side was coated with $LaNiO_3$ following exactly the same procedure.

Prcoesse of Pt Electrode Coating and Hot Poling: Pt top electrodes (20 mm by 10 mm) were coated on both sides of the PZT film via rf-sputtering (Kurt J. Lesker) and were patterned by a lift-off process. Alignment between the two electrodes was accomplished using a contact printer (Karl Suss MA/BA6). The dimensions of the PZT beam were made a little larger than the electrode size to avoid shorting from thermal or mechanical damage at the edge of beam induced by cutting the foil either with a laser or with scissors. It was found that cracks from the edge extended <200 µm into the beam. Finally, large-scale flexible bimorph {001} oriented PZT beams (dimension of 21.5 mm × 11.5 mm) were fabricated. The Ni substrate that served as the middle electrode was exposed by scratching the oxide layers with a razor blade. A resurrection treatment as described by Johnson-Wilke et al.[41] was used to remove or reduce any conducting pathways on these large area electrodes as shown in Figure 3a. The upper and lower PZT layers were then poled in opposite directions[42,43] using a high DC bias (3 × E_c, or 47 V) for 10 min at 150 °C. For poling, the bottom electrode (Ni substrate) was held at a positive voltage and the two Pt top electrodes were grounded. The opposing polarization directions between the two layers lead to an increase in the output voltage in series connection.[32]

Supporting Information

Supporting Information is available from the Wiley Online Library or from the author.

Acknowledgements

This work was supported by a National Security Science and Engineering faculty fellowship and the NSF ASSIST ERC (EEC-1160483). The authors gratefully acknowledge useful conversations with T. N. Jackson.

Received: March 5, 2016
Revised: April 29, 2016
Published online: June 7, 2016

[1] S. Priya, *J. Electroceram.* **2007**, *19*, 165.
[2] S.-G. Kim, S. Priya, I. Kanno, *MRS Bull.* **2012**, *37*, 1039.
[3] P. D. Mitcheson, E. M. Yeatman, G. K. Rao, A. S. Holmes, T. C. Green, *Proc. IEEE* **2008**, *96*, 1457.
[4] T. Starner, J. A. Paradiso, in *Low-Power Electronics Design* (Ed.: C. Piguet), CRC Press, Boca Raton, FL, USA **2004**, *Ch. 1*.
[5] L. Dhakar, H. Liu, F. E. H. Tay, C. Lee, *Sens. Actuators, A* **2013**, *199*, 344.
[6] T. Harigai, H. Adachi, E. Fuuii, *J. Appl. Phys.* **2010**, *107*, 096101.
[7] C. B. Yeager, S. Trolier-McKinstry, *J. Appl. Phys.* **2012**, *112*, 074107.
[8] K. Morimoto, I. Kanno, K. Wasa, H. Kotera, *Sens. Actuators, A* **2010**, *163*, 428.
[9] K.-I. Park, J. H. Son, G.-T. Hwang, C. K. Jeong, J. Ryu, M. Koo, I. Choi, S. H. Lee, M. Byun, Z. L. Wang, K. J. Lee, *Adv. Mater.* **2014**, *26*, 2514.
[10] S. Trolier-McKinstry, F. Griggio, C. Yeager, P. Jousse, D. Zhao, S. S. Bharadwaja, T. N. Jackson, S. Jesse, S. V. Kalinin, K. Wasa, *IEEE Trans. Ultrason. Ferroelectr. Freq. Control* **2011**, *9*, 1782.
[11] N. S. Hudak, G. G. Amatucci, *J. Appl. Phys.* **2008**, *103*, 101301.
[12] S. R. Anton, H. A. Sodano, *Smart Mater. Struct.* **2007**, *16*, R1.
[13] C. Yeager, *Ph.D. Thesis*, Penn State **2014**.
[14] S. Roundy, *J. Intell. Mater. Syst. Struct.* **2005**, *16*, 809.
[15] F. Calame, P. Muralt, *Appl. Phys. Lett.* **2007**, *90*, 062907.
[16] G. L. Brennecka, W. Huebner, B. A. Tuttle, P. G. Clem, *J. Am. Ceram. Soc.* **2004**, *87*, 1459.
[17] S.-C. Lin, W.-J. Wu, *J. Micromech. Microeng.* **2013**, *23*, 125028.
[18] S.-H Kim, H. Seo, S. Glinsek, Y. Kim, A. I. Kingon, presented at 16th US–Japan Seminar on Dielectric Piezoelectric Materials, Raleigh, NC, USA, November 2013.
[19] H. G. Yeo, S. Trolier-McKinstry, *J. Appl. Phys.* **2014**, *116*, 014105.
[20] B. A. Tuttle, J. A. Voight, D. C. Goodnow, D. L. Lamppa, T. J. Headley, M. O. Eatough, G. Zender, R. D. Nasby, S. M. Rodgers, *J. Am. Ceram. Soc.* **1993**, *76*, 1537.
[21] K. Wasa, T. Matsushima, H. Adachi, I. Kanno, H. Kotera, *J. Microelectromech. Syst.* **2012**, *12*, 451.
[22] R. Caliò, U. B. Rongala, D. Camboni, M. Milazzo, C. Stefanini, G. D. Petris, C. M. Oddo, *Sensors* **2014**, *14*, 4755.
[23] X. Ma, A. Wilson, C. D. Rahn, S. Trolier-McKinstry, *J. Vib. Acoust.* **2016**, *138*, 021005.
[24] C. L. Kuo, S. C. Lin, W. J. Wu, presented at 25th Int. Conf. on Adaptive Structures, Technologies, Hauge, Netherlands, October 2014.
[25] J.-I. Inoue, K. Kanda, T. Fujita, K. Maenaka, *J. Micromech. Microeng.* **2015**, *25*, 055001.
[26] S.-M. Ha, D.-H. Kim, H.-H. Park, T.-S. Kim, *Thin Solid Films* **1999**, *525*, 355.
[27] H. Suzuki, Y. Miwa, T. Naoe, H. Miyaraki, T. Ota, M. Fuji, M. Takahashi, *J. Eur. Ceram. Soc.* **2006**, *26*, 1953.
[28] T. Kobayashi, M. Ichiki, J. Tsaur, R. Maeda, *Thin Solid Films* **2005**, *489*, 74.
[29] R. W. Schwartz, J. A. Voigt, B. A. Tuttle, D. A. Payne, T. L. Reichert, R. S. DaSalla, *J. Mater. Res.* **1997**, *12*, 444.
[30] W. R. Cook Jr., D. A. Berlincourt, F. J. Scholz, *J. Appl. Phys.* **1963**, *34*, 1392.

[31] T. G. Kolie, *Phys. Rev. B* **1977**, *16*, 4872.
[32] R. Xu, A. Lei, C. Dahl-Petersen, K. Hansen, M. Guizzetti, K. Birkelund, E. V. Thomsen, O. Hansen, *Sens. Actuators, A* **2012**, *188*, 383.
[33] S. Leadenham, A. Erturk, *Smart Mater. Struct.* **2015**, *24*, 055021.
[34] D. Shen, J.-H. Park, J. Ajitsaria, S.-Y. Choe, H. C. Wikle, D.-J. Kim, *J. Micromech. Microeng.* **2008**, *18*, 055017.
[35] H.W. Kim, A. Batra, S. Priya, K. Uchino, D. Markley, R. E. Newham, H. F. Hofmann, *Jpn. J. Appl. Phys.* **2004**, *43*, 6178.
[36] R. Andosca, T. McDonald, V. Genova, S. Rosenberg, J. Keating, C. Benedixen, J. Wu, *Sens. Actuators, A* **2012**, *178*, 76.
[37] H. Durou, G. A. Ardilla-Rodriguez, A. Ramond, X. Dollat, C. Rossi, D. Esteve, *Power MEMS*, Leuven, Belgium **2010**, p. 27.
[38] T. Zawada, K. Hansen, R. Lou-Moeller, E. Ringgaard, T. Pedersen, E. V. Thomsen, *Proc. Eng.* **2010**, *5*, 1164.
[39] E. E. Aktakka, R. L. Peterson, K. Najafi, *16th Int. Solid-State Sensors, Actuators, and Microsystems Conf.* **2011**, DOI: 10.1109/TRANSDUCERS.2011.5969888.
[40] T. Ricart, P.-P. Lassagne, S. Boisseau, G. Despesse, A. Lefevre, C. Billard, S. Fanget, E. Defay, *IEEE Int. Ultras. Symp.* **2011**, DOI: 10.1109/ULTSYM.2011.0480.
[41] R. L. Johnson-Wilke, R. H. Wilke, V. Cotroneo, W. N. Davis, P. B. Reid, D. A. Schwartz, S. Trolier-McKinstry, *Proc. SPIE* **2012**, *8503*, 85030A.
[42] A. Erturk, D. J. Inman, *Smart Mater. Struct.* **2009**, *18*, 025009.
[43] A. Erturk, D. J. Inman, *Piezoelectric Energy Harvesting*, John Wiley & Sons, Chichester, UK **2011**.